Heliyon

Received:
14 August 2018
Revised:
1 February 2019
Accepted:
5 February 2019

Cite as: A. L. C. Conceição, K. Meehan, M. Antoniassi, M. Piacenti-Silva, M. E. Poletti. The influence of hydration on the architectural rearrangement of normal and neoplastic human breast tissues.
Heliyon 5 (2019) e01219.
doi: 10.1016/j.heliyon.2019.e01219

The influence of hydration on the architectural rearrangement of normal and neoplastic human breast tissues

A. L. C. Conceição [a,b,*], K. Meehan [c], M. Antoniassi [a], M. Piacenti-Silva [d], M. E. Poletti [e]

[a] *Universidade Tecnológica Federal do Paraná, Av. Sete de Setembro 3165, Curitiba, 80230-901, Paraná, Brazil*

[b] *Deutsches Elektronen-Synchrotron DESY, Notkestraße 85, D-22607, Hamburg, Germany*

[c] *School of Biomedical Sciences and Laboratory Medicine, The University of Western Australia, 35 Stirling Highway, Crawley, WA, 6009, Australia*

[d] *Departamento de Física, Faculdade de Ciências, UNESP, Av. Luiz Edmundo Carrijo Coube 14-01, 17033-360, Bauru, Brazil*

[e] *Departamento de Física, FFCLRP, Universidade de São Paulo, Ribeirão Preto, 14040-901, São Paulo, Brazil*

[*] Corresponding author.
E-mail address: alconceicao@utfpr.edu.br (A.L.C. Conceição).

Abstract

In adult women, the water-content represents between 50% and 70% of the mass in normal breast tissues and this percentage is increased within diseased tissues. Water molecules play an essential role in the structural organization of biological tissues such as breast. Then, in this study, we have investigated the influence of the water molecules on the breast tissue organization and their role on the hierarchical tissue rearrangement promoted by tumor growth.

SAXS and WAXS techniques were used to analyze healthy, benign and malignant human breast samples in native and lyophilized conditions. The scattering profiles in SAXS and WAXS regime of each tissue type in both conditions were compared in order to identify the structural transformation in these tissues and verify the water influence on the morphological arrangement of normal and pathological human breast tissues.

From SAXS, changes at the axial periodicity of collagen fibrils were revealed. Additionally, when the water content has removed a peak at $q = 4.17\ nm^{-1}$

https://doi.org/10.1016/j.heliyon.2019.e01219

(that was present only in pathological samples) shifted in opposite directions within benign and malignant lesions. From WAXS, water and fatty acids were identified within native samples. However, after freeze-drying, only the fat component was observed in the scattering profiles.

Therefore, when the water molecules were removed from the samples, structural changes associated with pathological progression were visible. From this, insights about their influence over the changes promoted by the tumor growth have been proposed. Finally, the findings of this study have the potential to provide valuable information to the development of new target therapy.

Keywords: Cancer research, Structural biology, Biomedical engineering, Molecular physics

1. Introduction

With the incidence of breast cancer increased over the last decade [1], many studies have sought to understand the morphological changes that occur in breast tissues due to carcinogenesis towards elucidating our understanding of disease development. Small (SAXS) and wide angle X-ray scattering (WAXS) are powerful techniques to reveal the structural arrangements of an object at the supramolecular and molecular scale, respectively.

Many works are employing SAXS and WAXS techniques to get information about the structural organization of healthy and pathological human breast tissue. SAXS analysis has been used by groups to reveal changes in collagen fibril d-spacing [2, 3, 4, 5] and variations in the amorphous scattering component [4, 5, 6, 7] that are related to breast cancer development. In addition, WAXS analysis has been used to identify structures like fatty acids and water molecules [8, 9, 10, 11] in an attempt to classify breast samples [10, 12, 13, 14].

Although previous studies present features that, in principle, are correlated to breast cancer growth, they do not provide insight regarding the changes in the functionality of the tissues dominated by the pathological cells. In adult women, the water-content represents between 50% and 70% of the mass in normal breast tissues [15], and this value is increased within pathological tissues [16]. From this, water molecules are supposed to play an essential role in the spatial arrangement of components within the breast and may subsequently influence metabolism within this tissue [17]. In this sense, recent studies have compared the structural arrangements of non-lyophilized (native) and lyophilized biological tissue by x-ray scattering techniques in order to evaluate the influence of the water molecules [18, 19, 20].

Desouky *et al.* (2001) [18] present WAXS profiles of several biological samples, including blood and its constituents, fat, muscle, proteins and DNA. In 2003 [20],

https://doi.org/10.1016/j.heliyon.2019.e01219

the same group characterized cirrhosis and hepatocellular carcinoma lyophilized samples by x-ray scattering. A peak of $q = 3.41\ nm^{-1}$ was observed within normal samples and this shifted to $q = 3.51\ nm^{-1}$ for cirrhosis cases and up to $3.61\ nm^{-1}$ for cases with hepatocellular carcinoma. These shifts were attributed to structural changes in serum proteins consistent with the onset and progression of cirrhosis to hepatocellular carcinoma.

Herein, we present SAXS and WAXS analyses of normal and pathological human breast tissues at native and lyophilized states. The results presented allow inference about the behavior of the water-soluble metabolites on the structural organization of the breast tissues and their role in the breast pathologies development.

2. Materials and methods

2.1. Breast tissue samples

Three human breast samples were analyzed in this study. They were obtained from reduction mammoplasties and prophylactic mastectomies from three female subjects at Clinics Hospital of Ribeirão Preto of the University of São Paulo (HC-FMRP/USP), Ribeirão Preto, Brazil. Two experts breast pathologists determined the pathological state of all tissues. The samples were fixed in formalin (4% formaldehyde in water) in order to preserve the structures within the tissues. Immediately before the measurements, the excess of formalin was withdrawn and each sample was cut into 2 mm thick portions to fit into the circular sample holder with 10mm of diameter and sandwiched by thin mica foils. After SAXS and WAXS measurements with the samples at native state, these samples were submitted to a lyophilization procedure using the lyophilizer Terroni® LS 3000. This process can be summarized as follows: (1) freezing the sample at $-50\ ^{\circ}C$ for 8h; (2) primary drying $-50\ ^{\circ}C$ for 48h; and (3) secondary drying at $25\ ^{\circ}C$ for 24h. The chamber pressure was maintained at 20Pa during the drying process. When the lyophilization process was over, the vials were immediately filled with nitrogen gas, sealed with rubber caps, and stored at $4\ ^{\circ}C$. The weights before and after the freeze-drying procedure were recorded and the wet-to-dry ratios calculated for each sample. At the moment of the measurements, the lyophilized samples were kept at room temperature in order to defrost.

2.1.1. Ethical approval

This study was approved by the Research Ethics Committee of the Clinics Hospital of Ribeirão Preto of the University of São Paulo (HC-FMRP/USP), Ribeirão Preto, Brazil, protocol no. 4305/2009, under the ethical guidelines of the Declaration of Helsinki and its revisions. Moreover, we declare that we have no access to patient data. In this study, we only collect the breast samples from a biobank with their

https://doi.org/10.1016/j.heliyon.2019.e01219

respective histopathological classifications. Therefore, by the ethical guidelines, no consent of the patients was needed.

2.2. SAXS measurements

The experiments were performed at the D02A-SAXS2 beamline in the National Synchrotron Light Laboratory in Campinas, Brazil. The experimental setup was mainly comprised by a source, a focused monochromator of Si (111) to provide an x-ray beam of wavelength 1.488 Å and a beam size of (1.0 × 0.5 mm) on the sample. Moreover, the experimental setup also consists of a sample-holder, a vacuum chamber to minimize air scattering and absorption losses, two systems of scatterer/detector (aluminum plate/NaI(Tl) detector) to determinate the sample attenuation and, finally a two-dimensional MarCCD 165 camera detector of 2048 × 2048 pixels, with resolution of 79μm per pixel. Two sample-detector distances were used (381 mm and 1602 mm), allowing to record the momentum transfer range of 0.150 $nm^{-1} < q(=4\pi.\sin(\theta/2)/\lambda) < 8.500\ nm^{-1}$, where θ is the scattering angle and λ is the wavelength. A beam stop of 6mm-diameter was inserted centralized and adjacent to the detector in order to avoid the saturation of the detector due to the primary intensity. In order to establish the correct reciprocal space scale of each image, a standard sample of Silver Behenate was used to calibrate and normalize the SAXS patterns for each sample-detector distance. The measured time was adjusted to get a maximum photon counting while not saturating the detector (300 s on average, depending on the electric current in the ring). Three SAXS images were acquired for each tissue sample, one being of the central portion and the others adjacent to this, separated by 2 mm. These images were summed in order to obtain an average scattering profile for the whole sample since each sample was histologically classified as representing the same tissue.

2.3. WAXS measurements

The angular distribution of photons scattered at WAXS region was measured using a powder diffractometer Siemens D5005 operating in back-reflection mode. The x-ray tube working at 40 kV and 30 mAs was equipped with a Cu anode ($K_\alpha = 8.04$keV) and Ni added filtration. A compensating divergence slit was used to keep the irradiated area constant at 6 mm × 10 mm. Moreover, a Söller slit was positioned between the compensating divergence slit and the sample, located on the central axis of the goniometer system, in order to minimize incident beam divergence. Between the sample and the detector system, other sets of Söller and compensating divergence slit were used to allow measurements within a small angular range around the desired scattering angle. The detector system consisted of a graphite monochromator and a scintillation detector of NaI. The monochromator was in order to accept scattered photons with the K_α energy of Cu and to exclude others energies (like

https://doi.org/10.1016/j.heliyon.2019.e01219

Compton in large angle and multiple scatter). Scattering angles from 4° up to 72° were scanned in steps of 1/3°, corresponding to q-range between 2.84 nm^{-1} and 47.90 nm^{-1}. A counting time of 30 s for each angular position was selected in order to provide a statistical uncertainty of less than 3%.

2.4. Data handling

SAXS images were azimuthally integrated using the software FIT2D [21] in order to extract the one-dimensional distribution of the scattered intensity. However, before the data reduction, detector artifacts were removed.

SAXS scattering profiles were obtained by applying some corrections and normalization, which are detailed in Conceição and coworkers [5]. This procedure can be summarized by the Eq. (1):

$$I_S(q) = I^*_{S+BG}(q) \cdot A_{S+BG} - I^*_{BG}(q) \cdot A_{BG} \quad (1)$$

where $I^*_{S+BG}(q)$and $I^*_{BG}(q)$ represents the sample plus background and the background scattering intensity, respectively. A_{S+BG} corresponds to the self-attenuation factor of sample plus background, while A_{BGi} the background attenuation factor. Sample self-attenuation factor was experimentally determined in fast measurements before the SAXS measurements, and it was considered constant for the whole q-range.

The scattering profiles obtained at the two distances used in this work were combined in order to obtain a unique scattering profile by the standard sample data in a common q interval to these distances.

Linear coherent scattering coefficients (μ_{CS}) were determined from WAXS data, all distribution of coherently scattered intensities measured were submitted to correction procedure and normalization, described in detail in our work [10]. Firstly, it was removed the photons originated from every other scattering sources that not the sample, $I_{M\_corr}(q)$. Next, correction due to polarization ($P(q)$) and sample self-attenuation and geometric effects ($A(q)$), where both were calculated using standard analytical functions [11, 22]. Finally, the data were normalized by using a scaling factor$K$. This factor is obtained by averaging the ratio between the experimental data and the theoretical one computed within the independent atomic model (IAM), using the composition and density values for the tissues at the native and lyophilized state shown in Table 1, for $q \geq 39\ nm^{-1}$. The Eq. (2) condenses this procedure:

$$\mu_{CS} = KI_{M\_corr}(q)P(q)^{-1}A(q)^{-1} \quad (2)$$

https://doi.org/10.1016/j.heliyon.2019.e01219

Table 1. Chemical and physical composition of the human breast tissues at native and lyophilized state.

Samples	State	H(%)	C(%)	N(%)	O(%)	Density (g/cm^3)
Normal Tissue	Native	10,7	63,0	3,0	23,3	0,91
	Lyophilized	10,8	70,8	0,8	17,6	0,78
Benign Lesion	Native	9,8	16,3	4,1	69,8	1,06
	Lyophilized	7,3	45,5	13,1	34,1	0,67
Malignant Lesion	Native	10,2	16,9	3,9	69,0	1,04
	Lyophilized	7,4	46,4	11,9	34,3	0,59

3. Results and discussion

After submission to the lyophilization process, the mass of the normal sample was reduced by 32%, while the benign and malignant lesions were reduced by 82% and 83%, respectively. This mass reduction is mostly due to the decrease of the oxygen content which also implies a reduction of the attenuation coefficient of those samples. Furthermore, the SAXS and WAXS scattering profiles also highlight the consequences of freeze-drying the specimens, Figs. 1 and 2 respectively.

3.1. SAXS scattering profiles

Fig. 1 shows the SAXS scattering profiles of normal (Fig. 1.a), benign (Fig. 1.b) and malignant (Fig. 1.c) human breast tissue at native and lyophilized state. These

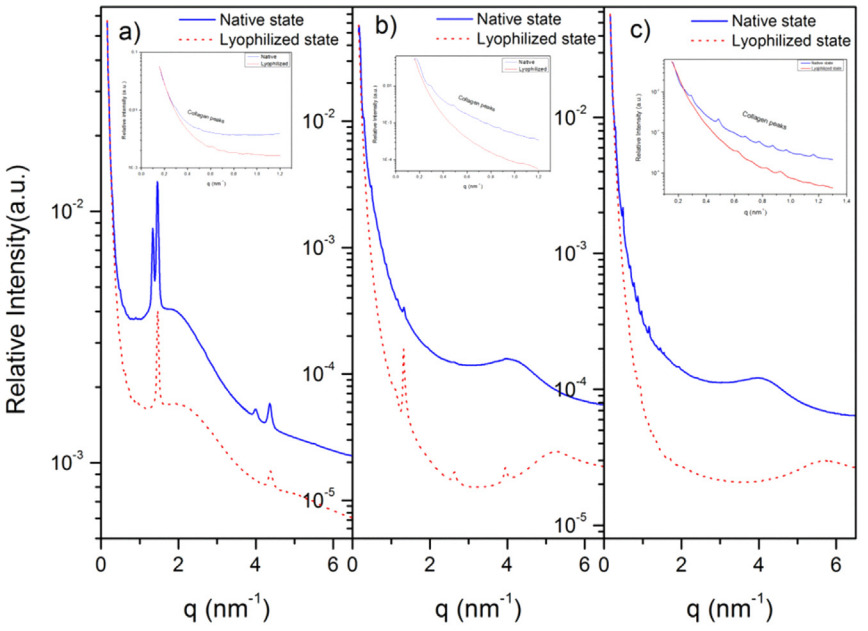

Fig. 1. Comparison of the SAXS scattering profiles of human breast tissues at the native and lyophilized state of a) normal tissue, b) benign lesion and c) malignant lesion. The inset in each figure shows in details the low q range, highlighting the collagen fibrils reflections.

https://doi.org/10.1016/j.heliyon.2019.e01219

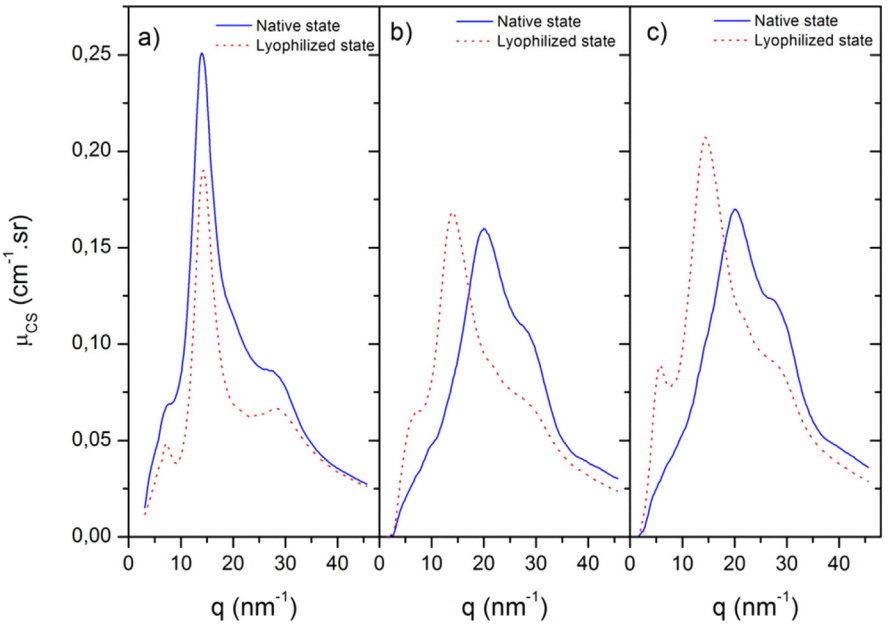

Fig. 2. Native and lyophilized scattering profiles of healthy and pathological human breast tissues at the WAXS region. a) normal tissue, b) benign lesion and c) malignant lesion.

scattering profiles can be divided into two regions: $q \leq 1.2$ nm^{-1} low SAXS and 1.2 nm^{-1}<q ≤ 6.5 nm^{-1} high SAXS.

Within the low region, all scattering profiles in the native state present the reflections corresponding to collagen fibrils, structures with d-spacing about 650Å, from 3rd order ($q = 0.29$ nm^{-1}) to 9th ($q = 0.87$ nm^{-1}) for normal, 10th ($q = 0.97$ nm^{-1}) for benign and 12th ($q = 1.16$ nm^{-1}) for the malignant lesion (shown in the inset of the Fig. 1.a, b and c respectively). A comparison of the scattering profiles at native and lyophilized states revealed a shift in each peak of collagen reflection, in agreement with Fratzl and Daxer [23]. However, we also observed a different shift specific to each type of tissue. On average, we detected a d-spacing reduction of 3.4 Å for normal, 1.5 Å for benign and 5.5 Å for the malignant lesion. This suggests that electron density is altered in a different way between normal, benign and malignant tissues and that the structure of collagen is different among physiologically normal and pathological states. Collagen fibrils are one of the main components of the extracellular matrix (ECM) and they behave as containing an anchoring structure. In principle, these fibrils are randomly orientated into the ECM; nevertheless, our data support the idea that tumor cells individually and actively realign collagen fibrils to facilitate local invasion by tumor cells from the primary tumor to the surrounding stroma [24, 25]. Our data also suggest that collagen fibril units are hydration-dependent, but considering the intensity at the lowest q-vector is visualized that the packing of collagen fibrils are not detectably altered by the changes in the hydration as also observed for collagen fibrils in corneal stroma [23]. This is because

https://doi.org/10.1016/j.heliyon.2019.e01219

collagen fibril rearrangement appeared to be similar among normal, benign and malignant tissues when in the native state but different when the water content was removed (lyophilized). The role of water in the process of collagen fibril structure in human breast tissue has not been previously investigated but may be related to the polarity of the water molecules. Concerning the amount of water in the breast, further investigations have to be carried out.

For the normal specimen in the high SAXS region (Fig. 1.a), two sharp peaks were observed at q = 1.33 nm^{-1} and q = 1.46 nm^{-1} in the native state. The first corresponds to structures with a periodic electron density of about 47Å and present harmonics of 3rd order (q = 3.99 nm^{-1}). However, these harmonics are lost in the lyophilized sample. This indicates that the structure with 47 Å of electron density may be due a hydrophilic structure and that when water is removed, this structure becomes unable to rearrange in a manner to produce a constructive scattering intensity. The second peak in Fig. 1.a is related to the lamellar phase of triacylglycerides [26], the main component of lipids. Both the 1st (q = 1.46 nm^{-1}) and 3rd (q = 4.38 nm^{-1}) order of lipids component are also present in the normal lyophilized sample (dot line). For the benign lesion, the structure with a periodic electron density of 47 Å was lightly observed by a small peak at of the peak at q = 1.33 nm^{-1}. After freeze-dried, the 2nd harmonic (q = 2.66 nm^{-1}) of the peak at q = 1.33 nm^{-1} was observed (Fig. 1.b) for the benign lesion. This behavior, distinct that observed for healthy tissue, may be associated with the dynamics of an altered ECM governed by benign differentiation. This may involve fibroblast activation and may, therefore, explain the observed increase in collagen fibrils density (i.e., desmoplasia). A broad peak at q = 4.17 nm^{-1} corresponding to the structure of 15.1 Å was visualized in both the benign (Fig. 1.b) and malignant lesions (Fig. 1.c) at the native state. However, when the water content was removed, this peak shifted to a higher q (5.63 nm^{-1}) for the malignant lesion (Fig. 1.c) compared with q = 5.19 nm^{-1} observed for the benign (Fig. 1.b). This shift may be associated with a structure present in the ECM that regulates tumor progression, e.g., a protein, but the identity is unclear. Triacylglycerides presence was weaker but still visible in the malignant scattering profile in both states native and lyophilized states (q = 1.46 nm^{-1}, Fig. 1.c). This fact corroborates with the histology of our malignant specimen classified as invasive ductal carcinoma, where the stroma undergoes desmoplastic reaction characterized by over-deposition of bundles of type I and III collagens, which means lower adipose content.

For the normal sample, the main peak at q = 1.46 nm^{-1} was observed in both the native and lyophilized states. In contrast, an amorphous peak at q = 4.17 nm^{-1} (15.1 Å) was observed in the benign and malignant samples at the native state that shifted to q = 5.19 nm^{-1} in the benign sample and q = 5.63 nm^{-1} in the malignant sample after lyophilization.

https://doi.org/10.1016/j.heliyon.2019.e01219

3.2. WAXS scattering profiles

Fig. 2 compares the WAXS scattering profiles of normal (Fig. 2.a), benign (Fig. 2.b) and malignant (Fig. 2.c) human breast tissue at native and lyophilized state. In Fig. 2.a one peak arises at $q = 6.8nm^{-1}$ for the lyophilized sample and is related to the structure of periodicity of 9.2 Å, but the origin of this remains unknown. A sharp peak at $q = 14.1\ nm^{-1}$ is easily identified at both states corresponding to structure with electron density correlation of 4.5 Å, previously shown be due to e intermolecular distance between the fatty acid molecules [27, 28, 29]. Moreover, a shoulder region near $q = 29\ nm^{-1}$ is present at both states of healthy tissue and is common to all scattering profiles at both states. Tartari et al. reported the same shoulder [27], tabulated the scattering profile of liquefied and filtered fat, and suggested that this represents intra-tissue heterogeneity. A different peak at $q = 20.2\ nm^{-1}$ was observed in the pathological lesions in the native states (Fig. 2.b and c), corresponding to the signal from the oxygen-oxygen electron density correlation between adjacent molecules on the tetrahedral structure of liquid water [8, 30]. Subsequently to the lyophilization, a shoulder around $q = 6.1\ nm^{-1}$ was observed on the benign WAXS profile (Fig. 2.b) and at $q = 5.6\ nm^{-1}$ for the malignant lesion (Fig. 2.c). These new structures shedding to light the distinct hierarchical arrangement between benign and malignant whose signal is probably suppressed by the water signal.

4. Conclusion

In this work, small and wide x-ray scattering techniques were used to investigate the role of water molecules on the structural organization of normal, benign and malignant human breast tissues.

At both SAXS and WAXS regions new peaks, not observed before according to the authors' knowledge probably due to their suppression by the water signal, enhanced the architectural arrangement between normal, benign and malignant tissues. Further studies are required to obtain additional information about these new structures.

Although previously reported that the dehydration process influences the collagen fibril structural units, findings from this study suggest no significant influence on the hierarchical arrangement of these fibrils. Thereby, the approach used in this study can be used for sample preparation in studies involving biological specimens by scattering techniques to minimize radiation damage.

Significance statement

Water-content represents between 50% and 70% of the mass in normal breast tissues in women and this percentage is increased within pathological tissues. Increased cell

https://doi.org/10.1016/j.heliyon.2019.e01219

hydration causes cancer not only by promoting cell division and oncogene expression, but also by inactivating genes inducing cell differentiation, and by preventing apoptosis. Nevertheless, how the water molecules influences on the hierarchical tissue arrangement transformation due to cancer initiation and growth is still unclear. Therefore, in this work, we investigated the tissue arrangement at a nanoscale level of normal, benign and malignant breast specimens by using two complementary X-ray elastic scattering techniques (WAXS and SAXS). We found out significant changes mainly related to collagen fibril unit and fatty acids which can be useful for cancer target therapy.

Declarations

Author contribution statement

Andre Conceicao: Conceived and designed the experiments; Performed the experiments; Analyzed and interpreted the data; Contributed reagents, materials, analysis tools or data; Wrote the paper.

Katie Meehan, Marina Piacenti-Silva: Analyzed and interpreted the data; Wrote the paper.

Marcelo Antoniassi: Performed the experiments; Analyzed and interpreted the data; Wrote the paper.

Martin Poletti: Conceived and designed the experiments; Performed the experiments; Contributed reagents, materials, analysis tools or data; Wrote the paper.

Funding statement

This work was supported by the São Paulo Research Foundation (FAPESP) under project number (2011/20632-6).

Competing interest statement

The authors declare no conflict of interest.

Additional information

No additional information is available for this paper.

Acknowledgements

The authors would like to acknowledge the support by the Brazilian agencies Fundação de Amparo à Pesquisa do Estado de São Paulo (FAPESP) and Conselho Nacional de Desenvolvimento Científico e Tecnológico (CNPq), as well as the

https://doi.org/10.1016/j.heliyon.2019.e01219

D02A-SAXS2 beamline staff for the help during the experiments in the National Synchrotron Light Laboratory (LNLS). In addition, we also would like to thank the Department of Pathology of the Hospital das Clínicas, Faculdade de Medicina de Ribeirão Preto, Brazil, for allows to collect of the human breast samples.

References

[1] WHO, Cancer, World Heal. Organ., 2017.

[2] R.A. Lewis, K.D. Rogers, C.J. Hall, E. Towns-Andrews, S. Slawson, A. Evans, S.E. Pinder, I.O. Ellis, C.R.M. Boggis, A.P. Hufton, D.R. Dance, Breast cancer diagnosis using scattered X-rays, J. Synchrotron Radiat. 7 (2000) 348−352.

[3] M. Fernández, J. Keyriläinen, R. Serimaa, M. Torkkeli, M.-L. Karjalainen-Lindsberg, M. Tenhunen, W. Thomlinson, V. Urban, P. Suortti, Small-angle x-ray scattering studies of human breast tissue samples, Phys. Med. Biol. 47 (2002) 577−592.

[4] S. Sidhu, K.K.W. Siu, G. Falzon, S. Nazaretian, S.A. Hart, J.G. Fox, B.J. Susil, R.A. Lewis, X-ray scattering for classifying tissue types associated with breast disease, Med. Phys. 35 (2008) 4660−4670.

[5] A.L.C. Conceição, M. Antoniassi, M.E. Poletti, Analysis of breast cancer by small angle X-ray scattering (SAXS), Analyst 134 (2009) 1077−1082.

[6] S. Sidhu, K.K.W. Siu, G. Falzon, S.A. Hart, J.G. Fox, R.A. Lewis, Mapping structural changes in breast tissue disease using x-ray scattering, Med. Phys. 36 (2009) 3211−3217.

[7] A.L.C. Conceição, M. Antoniassi, W. Geraldelli, M.E. Poletti, Mapping transitions between healthy and pathological lesions in human breast tissues by diffraction enhanced imaging computed tomography (DEI-CT) and small angle x-ray scattering (SAXS), Radiat. Phys. Chem. 95 (2014) 313−316.

[8] G. Kidane, R.D. Speller, G.J. Royle, A.M. Hanby, X-ray scatter signatures for normal and neoplastic breast tissues, Phys. Med. Biol. 44 (1999) 1791−1802.

[9] M.E. Poletti, O.D. Gonçalves, I. Mazzaro, X-ray scattering from human breast tissues and breast-equivalent materials, Phys. Med. Biol. 47 (2002) 47−63.

[10] O.R. Oliveira, A.L.C. Conceição, D.M. Cunha, M.E. Poletti, C.A. Pelá, Identification of neoplasias of breast tissues using a powder diffractometer, J. Radiat. Res. J. Radiat. Res. 49 (2008) 527−532.

[11] A.L.C. Conceiçao, M. Antoniassi, M.E. Poletti, Assessment of the differential linear coherent scattering coefficient of biological samples, Nucl. Instruments

https://doi.org/10.1016/j.heliyon.2019.e01219

Methods Phys. Res. Sect. A Accel. Spectrometers, Detect. Assoc. Equip. 619 (2010) 67–70.

[12] J.A. Griffiths, G.J. Royle, A.M. Hanby, J.A. Horrocks, S.E. Bohndiek, R.D. Speller, Correlation of energy dispersive diffraction signatures and microCT of small breast tissue samples with pathological analysis, Phys. Med. Biol. 52 (2007) 6151–6164.

[13] D.M. Cunha, O.R. Oliveira, C.A. Pérez, M.E. Poletti, X-ray scattering profiles of some normal and malignant human breast tissues, X Ray Spectrom. 35 (2006) 370–374.

[14] A.L.C. Conceição, M. Antoniassi, D.M. Cunha, A. Ribeiro-Silva, M.E. Poletti, Multivariate analysis of the scattering profiles of healthy and pathological human breast tissues, Nucl. Instruments Methods Phys. Res. Sect. A Accel. Spectrometers, Detect. Assoc. Equip. 652 (2011) 870–873.

[15] H.Q. Woodard, D.R. White, The composition of body tissues, Br. J. Radiol. 59 (1986) 1209–1218.

[16] S.C. Hagness, A. Taflove, J.E. Bridges, Two-dimensional FDTD analysis of a pulsed microwave confocal system for breast cancer detection: fixed-focus and antenna-array sensors, IEEE Trans. Biomed. Eng. 45 (1998) 1470–1479.

[17] R. Cooke, I.D. Kuntz, The properties of water in biological systems, Annu. Rev. Biophys. Bioeng. 3 (1974) 95–126.

[18] O.S. Desouky, W.M. Elshemey, N.S. Selim, A.H. Ashour, Analysis of low-angle x-ray scattering peaks from lyophilized biological samples, Phys. Med. Biol. 46 (2001) 2099–2106.

[19] W.M. Elshemey, O.S. Desouky, A.H. Ashour, Low-angle x-ray scattering from lyophilized blood constituents, Phys. Med. Biol. 46 (2001) 531–539.

[20] W.M. Elshemey, O.S. Desouky, M.S. Mohammed, A.A. Elsayed, M.E. Elhouseini, Characterization of cirrhosis and hepatocellular carcinoma using low-angle x-ray scattering signatures of serum, Phys. Med. Biol. 48 (2003) N239–N246.

[21] A.P. Hammersley, FIT2D : a multi-purpose data reduction, analysis and visualization program, J. Appl. Crystallogr. 49 (2016) 646–652.

[22] M.E. Poletti, O.D. Gonçalves, H. Schechter, I. Mazzaro, Precise evaluation of elastic differential scattering cross-sections and their uncertainties in X-ray scattering experiments, Nucl. Instrum. Methods Phys. Res. Sect. B Beam Interact. Mater. Atoms 187 (2002) 437–446.

https://doi.org/10.1016/j.heliyon.2019.e01219

[23] P. Fratzl, A. Daxer, Structural transformation of collagen fibrils in corneal stroma during drying. An x-ray scattering study, Biophys. J. 64 (1993) 1210−1214.

[24] P.P. Provenzano, D.R. Inman, K.W. Eliceiri, J.G. Knittel, L. Yan, C.T. Rueden, J.G. White, P.J. Keely, Collagen density promotes mammary tumor initiation and progression, BMC Med. 6 (11) (2008) 1−15.

[25] P.P. Provenzano, K.W. Eliceiri, J.M. Campbell, D.R. Inman, J.G. White, P.J. Keely, Collagen reorganization at the tumor-stromal interface facilitates local invasion, BMC Med. 4 (38) (2006) 1−16.

[26] J.A. Bouwstra, G.S. Gooris, F.E. Dubbelaar, M. Ponec, Phase behavior of lipid mixtures based on human ceramides: coexistence of crystalline and liquid phases, J. Lipid Res. 42 (2001) 1759−1770.

[27] A. Tartari, E. Casnati, C. Bonifazzi, C. Baraldi, Molecular differential cross sections for x-ray coherent scattering in fat and polymethyl methacrylate, Phys. Med. Biol. 42 (1997) 2551−2560.

[28] J. Kosanetzky, B. Knoerr, G. Harding, U. Neitzel, X-ray diffraction measurements of some plastic materials and body tissues, Med. Phys. 14 (1987) 526−532.

[29] J.R. Kanicky, D.O. Shah, Effect of degree, type, and position of unsaturation on the pKa of long-chain fatty acids, J. Colloid Interface Sci. 256 (2002) 201−207.

[30] T. Head-Gordon, M.E. Johnson, Tetrahedral structure or chains for liquid water, Proc. Natl. Acad. Sci. U. S. A 103 (2006) 7973−7977.

https://doi.org/10.1016/j.heliyon.2019.e01219